Seismoelectromagnetic homogeneous space Green's functions

Slob, Evert; Mulder, M.

DOI
10.1190/geo2015-0337.1

Publication date
2016

Document Version
Accepted author manuscript

Published in
Geophysics

Seismoelectromagnetic homogeneous space Green's functions

Evert Slob and Maarten Mulder

ABSTRACT

We present explicit expressions and the corresponding computer code for all homogeneous space Green's functions for coupled electromagnetic fields and poroelastic waves. The Green's functions are derived from the basic equations in closed-form in wavenumber-frequency and in space-frequency domains. They are given for point sources of any type. This adds several Green's functions to what has been published before. These Green's functions can be used in integral equation formulations, for numerical model validation, and for studying earthquake related electrokinetic effects. The wavenumber domain code for all Green's functions is given with the numerical test on the basic equations to demonstrate correctness. The numerical codes to compute them in space-frequency domain are also given. Numerical inverse FFT routine is used to provide space-time domain results. At seismic frequencies the fast P-wave is radiated with the largest amplitude in all fields, except for the magnetic fields where no P-waves are generated. At ultrasonic frequencies and in the particle and filtration velocity fields generated by an electric current source the slow P-wave has the strongest amplitude. In the filtration velocity and particle velocity the slow P-wave is, respectively, three orders and one order of magnitude stronger than the fast P-wave.

INTRODUCTION

A macroscopic model describing the coupling of electromagnetic fields and elastic waves in porous media has been derived by Pride (1994). The model consists of coupling between Maxwell's electromagnetic field equations and Biot's equations for poroelastic waves. The coupling mechanism lies in the transport equations that are part of the Maxwell and Biot equations. The actual model parameters are subject to assumptions on the physical mechanisms underlying the model. In Pride's model the assumptions are that there are no wave induced diffusion effects, chemical gradients are absent so that no free charges are induced on the grain surfaces, the pore fluids are ideal electrolytes, there is no grain-scale wave scattering, all disturbances induce linear effects only, and piezo or other anisotropy effects are absent. Pride's postulations for the frequency dependent coupling coefficient, the dynamic permeability, and electric conductivity are not necessarily the best ones. An alternative formulation can be found in Revil and Mahardika (2013), which allows for unsaturated porous media, and a recent development has paved the way to include two immiscible fluids in the pore volume (Jardani and Revil, 2015). Two kinds of seismoelectric effects are known. The first kind is based on the the electric field changes while an elastic disturbances passes, because that disturbance creates resistivity changes within the elastic disturbance. The setup was made with two electrodes between which a constant current runs and the electric potential difference is measured while an elastic waves passes by the electrodes (Thompson, 1936). The idea was that direct waves have different effects than reflections due to

their large difference in apparent horizontal slownesses, which could be used to discriminate between them in a measurement. The second kind is what we now know as the coupling effect where the electric and magnetic fields are coupled (Ivanov, 1940; Martner and Sparks, 1959). Although the coupling effect is known for a long time, the seismoelectromagnetic method is not routinely used in exploration geophysical activities. Field trials are reported on massive sulfide and hydrocarbon deposits (Kepic et al., 1995; Thompson et al., 2007) and for near surface investigations (Butler et al., 1996; Mikhailov et al., 2000; Garambois and Dietrich, 2001). The electrokinetic effect has been proposed as a mechanism for electromagnetic fields generated during earthquakes (Karakelian et al., 2002), but no evidence was given. Laboratory experiments at ultrasonic frequencies have been reported where the coupled electromagnetic and elastic responses were observed (Zhu et al., 1999; Zhu and Toksöz, 2005; Bordes et al., 2006; Zhu et al., 2008; Bordes et al., 2008). Experiments and numerical validation of experimental results have been reported successful (Schakel et al., 2011a,b). Several numerical models have been developed for 2D media (Han and Wang, 2001; Haines and Pride, 2006; Zyserman et al., 2010; Guan et al., 2013; Kroeger et al., 2014). Recently, dedicated data processing techniques were developed (Haines et al., 2007; Warden et al., 2012). Inversion and laboratory experiments with successful inversion results have also been developed (Mahardika et al., 2012; Haas et al., 2013). Laboratory observed transfer functions as a function of water saturation have been reported in Bordes et al. (2015).

The first who published homogeneous space Green's functions were Pride and Haartsen (1996) who derived closed-form expressions for the electric field and the particle displacement and filtration displacement fields generated by an electric current and forces acting on the bulk and fluid, respectively. For these sources they continued by modeling point source responses in a horizontally stratified medium (Haartsen and Pride, 1997). Haartsen et al. (1998) derived expressions for the streaming currents generated by point sources of vertical force and volume injection rate in a homogeneous porous medium. Curiously, the authors do not present possible closed-form expressions, but give their results as Hankel transformations, and they do not refer back to the closed-form expression given by Pride and Haartsen in 1996. Gao and Hu (2010) derived closed form expressions for the magnetic field generated by the three sources used in Pride and Haartsen (1996). They also stated that not all sources can be represented by point sources, such as an explosive source or a moment tensor source. They derived closed-form expressions for the electric and magnetic fields generated by a moment tensor source. They did not introduce the source as a point source in the basic equations, but used results from elastodynamic theory to introduce moment tensor responses from known Green's functions for a force source active on the bulk. This is not entirely correct for the coupled seismic and electromagnetic model, because the influence of a force acting on the fluid should also be incorporated in the response to a moment tensor. They continued to model the response of a homogeneous halfspace in which a finite fault generated a seismoelectromagnetic response (Hu and Gao, 2011). Here we give a proper source model that can be used as a source mechanism for earthquakes. Even though our model is a single homogeneous medium and the source is a point source, the way the source is incorporated allows for similar implementations in more complicated models. Garambois and Dietrich (2002) also developed a code for modeling point source responses in horizontally stratified media based on the scattering matrix formulation; Ren et al. (2010) developed a layered media model and code based on a slightly different implementation. Finally it is worth mentioning that when the coupling coefficient is set to

zero, the Green's functions for the bulk stress, the acoustic pressure, particle and filtration velocity fields generated by force sources acting on the bulk and fluid as well as deformation rate and volume injections rate sources are obtained and be compared to those given in Karpfinger et al. (2009). The equations developed here can be used in modeling when a primary-secondary formulation is used, such as in integral equation modeling, and to test numerical results of other codes when they model the direct fields numerically.

In this paper we derive closed form expressions for all Green's functions for fields generated by any type of source in a homogeneous medium. This is done by putting a source term in each of the basic equations whereby the explosion source is modeled as a volume injection rate and a moment tensor source is modeled as a deformation rate source. They both occur in the tensor and scalar deformation equations. There are six types of fields and six types of sources. We give the closed-form expressions of all Green's functions in the wavenumber-frequency domain. Ten tensor Green's functions are found with field-source dependent coefficients. The numerical codes are written Matlab and compute all fields for each source type*. In these codes the six basic equations are used to numerically validate the obtained Green's functions. These results are shown when the available codes are run, but these results are not shown here in the paper. We then evaluate the inverse spatial Fourier transformations in general terms and use the source-field coefficients in the closed-form expressions in the space-frequency domain Green's function expressions. We show some numerical results in the space-time domain and provide the numerical codes for all fields generated by any source type*. We briefly discuss the results of the space-time behavior.

BASIC EQUATIONS

The basic equations for the coupled electromagnetic fields and elastic waves in a homogeneous porous medium can be written as three sets of coupled equations (Pride, 1994; Revil and Mahardika, 2013). The equations as they are given here below we assume linear medium responses so that linear macroscopic theory for isotropic media is valid. We develop the equations in the three-dimensional spatial-Fourier time-Laplace transformed domain. We use the following transformations. The time-Laplace transformation of a field quantity $F(\boldsymbol{x},t)$ is given by

$$\hat{F}(\boldsymbol{x},s)=\int_{t=0}^{\infty}F(\boldsymbol{x},t)\exp(-st)\mathrm{d}t, \tag{1}$$

where t denotes time and the Laplace transformation parameter s can be chosen as $s=\mathrm{i}\omega$ to reduce it to a temporal Fourier transformation and where i denotes the imaginary unit. The three-dimensional spatial Fourier transformation of a quantity $\hat{F}(\boldsymbol{x},s)$ is given by

$$\breve{F}(\boldsymbol{k},s)=\int_{\boldsymbol{x}\in\mathbf{R}^3}\hat{F}(\boldsymbol{x},s)\exp(\mathrm{i}k_mx_m)\mathrm{d}\boldsymbol{x}. \tag{2}$$

The Cartesian vector components of the wavenumber vector $\boldsymbol{k}$ are denoted k_m and x_m denotes the coordinates of the position vector $\boldsymbol{x}$. We use Einstein's summation convention for repeated lower case Latin subscripts in the range from 1 to 3, e.g., $k_mx_m=k_1x_1+$

*Peer-reviewed code related to this article can be found at http://software.seg.org/2016/0003.

$k_2x_2 + k_3x_3$. The first basic equations are the two modified Maxwell equations (Schoemaker et al., 2012),

$$\epsilon_{kmp}\mathrm{i}k_m\breve{H}_p + \varsigma\breve{E}_k + s\rho^{(E)}\hat{L}\breve{w}_k = -\breve{J}_k^{(e)}, \tag{3}$$

$$-\epsilon_{jnr}\mathrm{i}k_n\breve{E}_r + \zeta\breve{H}_j = -\breve{J}_j^{(m)}, \tag{4}$$

where ϵ_{kmj} is the anti-symmetric tensor of rank three, $\epsilon_{ijk} = (i-j)(j-k)(k-i)/2$. The vector components of the electric and magnetic field vectors are given by $\breve{E}_k, \breve{H}_j$, whereas $\breve{J}_k^{(e)}, \breve{J}_j^{(m)}$ denote the electric and magnetic current sources; $\breve{w}_i$ is the filtration velocity vector, given by $\breve{w}_i = \phi(\breve{v}_i^{(f)} - \breve{v}_i)$, in which ϕ denotes porosity, and $\breve{v}_i^{(f)}, \breve{v}_i$ denote the particle velocity vector components in the fluid and solid, respectively. The medium parameters are given by,

$$\varsigma = \eta^{(e)} - s\rho^{(E)}\hat{L}^2, \qquad \eta^{(e)} = \hat{\sigma}^{(e)} + s\varepsilon, \tag{5}$$

$$\zeta = \hat{\sigma}^{(m)} + s\mu, \qquad \rho^{(E)} = \eta/(s\hat{k}), \tag{6}$$

where $\hat{\sigma}^{(e)}, \hat{\sigma}^{(m)}$ are the generalized electric and magnetic conductivity, which include electric and magnetic dissipation and polarization effects and ε, μ are the electric permittivity and magnetic permeability which account for propagation effects; η is viscosity, $\hat{k}$ is the dynamic permeability; $\hat{L}$ is the coupling coefficient. The equations of motion are given by

$$s\rho\breve{v}_i + s\rho^{(f)}\breve{w}_i + \mathrm{i}k_j(\breve{\tau}_{ij} + \breve{\tau}_{ji})/2 = \breve{f}_i, \tag{7}$$

$$s\rho^{(f)}\breve{v}_i + s\rho^{(E)}(\breve{w}_i - L\breve{E}_i) - \mathrm{i}k_i\breve{p} = \breve{f}_i^{(f)}, \tag{8}$$

where $\rho, \rho^{(f)}$ are the mass density of the bulk and fluid, respectively, $\breve{\tau}_{ij}, \breve{p}$ denote the components of the stress tensor and acoustic pressure, and $\breve{f}, \breve{f}^{(f)}$ represent the components of the force source vectors acting on the bulk and fluid, respectively. The deformation equations are given by

$$-s\breve{\tau}_{ij} - c_{ijkl}\mathrm{i}k_l\breve{v}_k - C\delta_{ij}\mathrm{i}k_m\breve{w}_m = c_{ijkl}\breve{h}_{kl} + C\delta_{ij}\breve{q}, \tag{9}$$

$$s\breve{p} - C\mathrm{i}k_m\breve{v}_m - M\mathrm{i}k_n\breve{w}_n = C\breve{h}_{ii} + M\breve{q}, \tag{10}$$

where δ_{ij} denotes the components of the unit matrix; C, M are stiffness parameters of the porous solid and c_{ijkl} is the stiffness tensor, given by

$$c_{ijkl} = (K_G - 2G^{(fr)}/3)\delta_{ij}\delta_{kl} + G^{(fr)}(\delta_{ik}\delta_{jl} + \delta_{il}\delta_{jk}), \tag{11}$$

in which $K_G, G^{(fr)}$ are the bulk and shear moduli of the porous solid. The deformation and volume injection rate sources are given by $\breve{h}_{ij}, \breve{q}$, respectively. The coupled seismic and electromagnetic wavefield has four different types of wavefields characterised by the slow and fast P-waves, the seismic shear wave, and the electromagnetic field. Hence we need to find the solution for these waves and fields. Because of the large number of coupled equations this is lengthy, yet straightforward. A relatively easy way is to eliminate the magnetic field, bulk stress, filtration velocity, and acoustic pressure, leaving a coupled system of equations for the electric field and the particle velocity in the solid. The detailed derivation of these two coupled equations is given in Appendix A and the solution procedure is given in Appendix

B. The fields can then be expressed with the aid of Green's functions and the sources as

$$\begin{pmatrix} \breve{v}_i \\ \breve{E}_i \\ \breve{w}_i \\ \breve{H}_i \\ \breve{p} \\ \breve{\tau}_{ir} \end{pmatrix} = \begin{pmatrix} \breve{G}^{vf}_{ij} & \breve{G}^{ve}_{ij} & \breve{G}^{vff}_{ij} & \breve{G}^{vm}_{ij} & \breve{G}^{vq}_{i} & \breve{G}^{vh}_{ikl} \\ \breve{G}^{ef}_{ij} & \breve{G}^{ee}_{ij} & \breve{G}^{eff}_{ij} & \breve{G}^{em}_{ij} & \breve{G}^{eq}_{i} & \breve{G}^{eh}_{ikl} \\ \breve{G}^{wf}_{ij} & \breve{G}^{we}_{ij} & \breve{G}^{wff}_{ij} & \breve{G}^{wm}_{ij} & \breve{G}^{wq}_{i} & \breve{G}^{wh}_{ikl} \\ \breve{G}^{mf}_{ij} & \breve{G}^{me}_{ij} & \breve{G}^{mff}_{ij} & \breve{G}^{mm}_{ij} & \breve{G}^{mq}_{i} & \breve{G}^{mh}_{ikl} \\ \breve{G}^{pf}_{j} & \breve{G}^{pe}_{j} & \breve{G}^{pff}_{j} & \breve{G}^{pm}_{j} & \breve{G}^{pq} & \breve{G}^{ph}_{kl} \\ \breve{G}^{\tau f}_{irj} & \breve{G}^{\tau e}_{irj} & \breve{G}^{\tau ff}_{irj} & \breve{G}^{\tau m}_{irj} & \breve{G}^{\tau q}_{ir} & \breve{G}^{\tau h}_{irkl} \end{pmatrix} \begin{pmatrix} \breve{f}_j \\ \breve{J}^{(e)}_j \\ \breve{f}^{(f)}_j \\ \breve{J}^{(m)}_j \\ \breve{q} \\ \breve{h}_{kl} \end{pmatrix}, \tag{12}$$

where the Green's functions have superscripts that relate to the field and source types, e.g. $\breve{G}^{vff}_{ij}$ denotes the tensor components of the particle velocity Green's function component i generated by a force with component j exerted on the fluid and $\breve{G}^{mh}_{ikl}$ denotes the tensor components of the magnetic field Green's function component i generated by a deformation rate source with components kl exerted on the bulk. These Green's functions are given in closed form in the wavenumber-frequency and space-frequency domains in the following two sections, respectively.

WAVENUMBER DOMAIN GREEN'S FUNCTIONS

The Green's functions for the particle velocity and the electric field are derived in detail in Appendix B and all others follow from these. For the Green's functions we use tensor descriptions as outlined in Appendix B. They are given by

$$\breve{G}^{rs}_{ij} = \breve{K}^{rs}_{SS}\left(\frac{k_ik_j}{k^2}-\delta_{ij}\right)\breve{G}^{SS} + \breve{K}^{rs}_{PP}\frac{k_ik_j}{k^2}\breve{G}^{PP}, \tag{13}$$

$$\breve{G}^{ps}_{i} = -\breve{K}^{ps}_{PP}\mathrm{i}k_i\breve{G}^{PP}, \tag{14}$$

$$\breve{G}^{ms}_{ij} = -\breve{K}^{ms}_{SS}\epsilon_{imj}\mathrm{i}k_m\breve{G}^{SS}, \tag{15}$$

$$\begin{aligned}\breve{G}^{\tau s}_{ijk} = &-\breve{K}^{\tau s}_{SS}\left[\left(\frac{k_ik_k}{k^2}-\delta_{ik}\right)\mathrm{i}k_j + \left(\frac{k_jk_k}{k^2}-\delta_{jk}\right)\mathrm{i}k_i\right]\breve{G}^{SS} \\ &- \breve{K}^{\tau s}_{PP}\left(\frac{k_ik_j}{k^2}-\delta_{ij}\right)\mathrm{i}k_k - \breve{N}^{\tau s}_{PP}\delta_{ij}\mathrm{i}k_k,\end{aligned} \tag{16}$$

$$\breve{G}^{pq} = \breve{K}^{pq}_{PP}\breve{G}^{PP}, \tag{17}$$

$$\breve{G}^{mq}_{i} = \breve{G}^{pm}_{i} = 0, \tag{18}$$

$$\breve{G}^{\tau q}_{ij} = -\breve{K}^{\tau q}_{PP}k^2\left(\frac{k_ik_j}{k^2}-\delta_{ij}\right)\breve{G}^{PP} + \breve{N}^{\tau q}_{PP}\breve{G}^{PP}\delta_{ij}, \tag{19}$$

$$\breve{G}^{mm}_{ij} = -\breve{K}^{mm}_{SS}\left(\zeta^{-1}k_ik_j + \eta^{(e)}\delta_{ij}\right)\breve{G}^{SS} + \breve{N}^{mm}_{SS}\breve{G}^{SS}\delta_{ij}, \tag{20}$$

$$\breve{G}^{\tau m}_{ijk} = -\breve{K}^{\tau m}_{SS}\left(\epsilon_{imk}k_mk_j + \epsilon_{jmk}k_mk_i\right)\breve{G}^{SS}, \tag{21}$$

$$\breve{G}^{\tau h}_{ijkl} = \breve{K}^{\tau h}_{PP}\left[\delta_{ij}\left(\frac{k_k k_l}{k^2}-\delta_{kl}\right)+\left(\frac{k_i k_j}{k^2}-\delta_{ij}\right)\delta_{kl}\right]\breve{G}^{PP}$$
$$+\breve{Q}^{\tau h}_{PP}\left(\frac{k_i k_j}{k^2}-\delta_{ij}\right)\left(\frac{k_k k_l}{k^2}-\delta_{kl}\right)\breve{G}^{PP}+\breve{N}^{\tau h}_{PP}\breve{G}^{PP}\delta_{ij}\delta_{kl}$$
$$-\breve{K}^{\tau h}_{SS}\left[\left(\left(\frac{k_i k_k}{k^2}-\delta_{ik}\right)k_j k_l+\left(\frac{k_i k_l}{k^2}\delta_{il}\right)k_j k_k+\left(\frac{k_j k_k}{k^2}-\delta_{jk}\right)k_i k_l\right.$$
$$\left.+\left(\frac{k_j k_l}{k^2}\delta_{jl}\right)k_i k_k\right]\breve{G}^{SS}-\frac{H-2G^{(fr)}}{s}\delta_{ij}\delta_{kl}-\frac{G^{(fr)}}{s}(\delta_{ik}\delta_{jl}+\delta_{il}\delta_{jk}), \tag{22}$$

where the superscript ^{s} in equations 13-16 can be $s=\{f,e,ff\}$ and superscript ^{r} in equation 13 can be $r=\{v,e,w\}$. Equation 13 contains the Green's functions derived in Pride and Haartsen (1996) and equation 15 is given in Gao and Hu (2010), while the others are new. It can be observed that the direct source terms are still present in equation 22. These could be eliminated by reworking the other parts, but that does not lead to a more comprehensive result. For the Green's functions the following source-receiver reciprocity relations hold

$$\breve{G}^{ve}_{ij}(\boldsymbol{k},s)=\breve{G}^{ef}_{ji}(-\boldsymbol{k},s), \qquad \breve{G}^{vq}_{i}(\boldsymbol{k},s)=-\breve{G}^{pf}_{i}(-\boldsymbol{k},s), \tag{23}$$
$$\breve{G}^{vff}_{ij}(\boldsymbol{k},s)=\breve{G}^{wf}_{ji}(-\boldsymbol{k},s), \qquad \breve{G}^{eq}_{i}(\boldsymbol{k},s)=-\hat{G}^{pe}_{i}(-\boldsymbol{k},s), \tag{24}$$
$$\breve{G}^{eff}_{ij}(\boldsymbol{k},s)=\breve{G}^{we}_{ji}(-\boldsymbol{k},s), \qquad \breve{G}^{wq}_{i}(\boldsymbol{k},s)=-\breve{G}^{pff}_{i}(-\boldsymbol{k},s), \tag{25}$$
$$\breve{G}^{vm}_{ij}(\boldsymbol{k},s)=-\breve{G}^{mf}_{ji}(-\boldsymbol{k},s), \qquad \breve{G}^{vh}_{ijk}(\boldsymbol{k},s)=\breve{G}^{\tau f}_{kji}(-\boldsymbol{k},s), \tag{26}$$
$$\breve{G}^{em}_{ij}(\boldsymbol{k},s)=-\breve{G}^{me}_{ji}(-\boldsymbol{k},s), \qquad \breve{G}^{eh}_{ijk}(\boldsymbol{k},s)=\breve{G}^{\tau e}_{kji}(-\boldsymbol{k},s), \tag{27}$$
$$\breve{G}^{wm}_{ij}(\boldsymbol{k},s)=-\breve{G}^{mff}_{ji}(-\boldsymbol{k},s), \qquad \breve{G}^{wh}_{ijk}(\boldsymbol{k},s)=\breve{G}^{\tau ff}_{kji}(-\boldsymbol{k},s), \tag{28}$$
$$\breve{G}^{ph}_{ij}(\boldsymbol{k},s)=-\breve{G}^{\tau q}_{ji}(-\boldsymbol{k},s), \qquad \breve{G}^{mh}_{ijk}(\boldsymbol{k},s)=-\breve{G}^{\tau m}_{kji}(-\boldsymbol{k},s). \tag{29}$$

The scalar transversal and longitudinal wave Green's functions are given by

$$\breve{G}^{SS}=\frac{1}{(k^2+\gamma_S^2)}-\frac{1}{(k^2+\gamma_{EM}^2)}, \tag{30}$$
$$\breve{G}^{PP}=\frac{1}{(k^2+\gamma_{Pf}^2)}-\frac{1}{(k^2+\gamma_{Ps}^2)}, \tag{31}$$

in which $\gamma_S,\gamma_{EM},\gamma_{Pf},\gamma_{Ps}$ denote the spherical wavenumbers of the shear wave, electromagnetic field, and the fast and slow P-waves, respectively, given in equations B-9, B-10, B-12, and B-13.

The coefficients for the fields generated by a force source acting on the bulk are given by

$$\breve{K}^{vf}_{SS}=-\frac{s}{G^{(fr)}}\frac{\zeta\eta^{(e)}+k^2}{\gamma_{EM}^2-\gamma_S^2}, \tag{32}$$
$$\breve{K}^{vf}_{PP}=\left(\frac{sM}{HM-C^2}\right)\frac{s^2\rho^{(E)}\eta^{(e)}/(M\varsigma)+k^2}{\gamma_{Ps}^2-\gamma_{Pf}^2}, \tag{33}$$
$$\breve{K}^{ef}_{SS}=-\frac{s^2\rho^{(f)}\zeta\hat{L}}{G^{(fr)}}\frac{1}{\gamma_{EM}^2-\gamma_S^2}, \tag{34}$$
$$\breve{K}^{ef}_{PP}=\left(\frac{s^2\rho^{(E)}\hat{L}C}{(HM-C^2)\varsigma}\right)\frac{s^2\rho^{(f)}/C+k^2}{\gamma_{Ps}^2-\gamma_{Pf}^2}. \tag{35}$$

$$\breve{K}_{SS}^{wf} = \frac{s\rho^{(f)}}{\rho^{(E)}G^{(fr)}}\frac{\zeta\varsigma + k^2}{\gamma_{EM}^2 - \gamma_S^2}, \tag{36}$$

$$\breve{K}_{PP}^{wf} = -\left(\frac{sC}{HM - C^2}\right)\frac{s^2\rho^{(f)}/C + k^2}{\gamma_{Ps}^2 - \gamma_{Pf}^2}. \tag{37}$$

$$\breve{K}_{PP}^{pf} = -\left(\frac{s^2}{HM - C^2}\right)\frac{\rho^{(E)}\eta^{(e)}C/\varsigma - \rho^{(f)}M}{\gamma_{Ps}^2 - \gamma_{Pf}^2}, \tag{38}$$

$$\breve{K}_{SS}^{mf} = -\frac{s^2\rho^{(f)}\hat{L}}{G^{(fr)}}\frac{1}{\gamma_{EM}^2 - \gamma_S^2}, \tag{39}$$

$$\breve{K}_{SS}^{\tau f} = -\frac{\zeta\eta^{(e)} + k^2}{\gamma_{EM}^2 - \gamma_S^2}, \tag{40}$$

$$\breve{K}_{PP}^{\tau f} = 2\left(\frac{G^{(fr)}M}{HM - C^2}\right)\frac{s^2\rho^{(E)}\eta^{(e)}/(M\varsigma) + k^2}{\gamma_{Ps}^2 - \gamma_{Pf}^2}, \tag{41}$$

and

$$\breve{N}_{PP}^{\tau f} = \frac{s^2(\rho^{(E)}H\eta^{(e)}/\varsigma - \rho^{(f)}C)/(HM - C^2) + k^2}{\gamma_{Ps}^2 - \gamma_{Pf}^2}. \tag{42}$$

The coefficients for the fields generated by an electric current source are given by

$$\breve{K}_{SS}^{ee} = \zeta\frac{s^2\rho^{(c)}/G^{(fr)} + k^2}{\gamma_{EM}^2 - \gamma_S^2}, \tag{43}$$

$$\breve{K}_{PP}^{ee} = \left(\frac{(s\rho^{(E)}\hat{L})^2 sH}{(HM - C^2)\varsigma^2}\right)\frac{s^2\rho/H + k^2}{\gamma_{Ps}^2 - \gamma_{Pf}^2} - \frac{\breve{G}^{PP}}{\varsigma}. \tag{44}$$

$$\breve{K}_{SS}^{we} = \zeta\hat{L}\frac{s^2\rho/G^{(fr)} + k^2}{\gamma_{EM}^2 - \gamma_S^2}, \tag{45}$$

$$\breve{K}_{PP}^{we} = -\left(\frac{s^2\rho^{(E)}\hat{L}H}{(HM - C^2)\varsigma}\right)\frac{s^2\rho/H + k^2}{\gamma_{Ps}^2 - \gamma_{Pf}^2}, \tag{46}$$

$$\breve{K}_{PP}^{pe} = \frac{s\rho^{(E)}\hat{L}}{\varsigma}\frac{s^2(\rho M - \rho^{(f)}C) + k^2}{\gamma_{Ps}^2 - \gamma_{Pf}^2}, \tag{47}$$

$$\breve{K}_{SS}^{me} = \frac{s^2\rho^{(c)}/G^{(fr)} + k^2}{\gamma_{EM}^2 - \gamma_S^2}, \tag{48}$$

$$\breve{K}_{SS}^{\tau e} = -\frac{s\rho^{(f)}\hat{L}\zeta}{\gamma_{EM}^2 - \gamma_S^2}, \tag{49}$$

$$\breve{K}_{PP}^{\tau e} = 2\left(\frac{s\rho^{(E)}\hat{L}G^{(fr)}C}{(HM - C^2)\varsigma}\right)\frac{s^2\rho^{(f)}/C + k^2}{\gamma_{Ps}^2 - \gamma_{Pf}^2}, \tag{50}$$

$$\breve{N}_{PP}^{\tau e} = \left(\frac{s\rho^{(E)}\hat{L}}{(HM - C^2)\varsigma}\right)\frac{s^2(\rho^{(f)}H - \rho C)}{\gamma_{Ps}^2 - \gamma_{Pf}^2}, \tag{51}$$

Notice that in equation 44 a separate factor $\breve{G}^{PP}/\varsigma$ is present. Although this term is absent in Pride and Haartsen (1996) it is necessary, which can be seen by taking the limit in the wavenumber-frequency domain of $\hat{L} \to 0$. It is not required in the space-frequency domain in the same limit, showing that the simple pole at $k = 0$ does not give a contribution to the space-domain result as explained in Appendix B. The coefficients for the particle velocity generated by an electric current source are omitted, because these can be obtained from the reciprocity relations.

The coefficients for the fields generated by a force acting on the fluid, which cannot be directly found from reciprocity, are given by

$$\breve{K}_{SS}^{wff} = -\frac{1}{s\rho^{(E)}} \frac{(s^2\rho/G^{(fr)} + k^2)(\zeta\varsigma + k^2)}{\gamma_{EM}^2 - \gamma_S^2}, \tag{52}$$

$$\breve{K}_{PP}^{wff} = \left(\frac{sH}{HM - C^2}\right) \frac{s^2\rho/H + k^2)}{\gamma_{Ps}^2 - \gamma_{Pf}^2}, \tag{53}$$

$$\breve{K}_{PP}^{pff} = -\frac{s^2(\rho M - \rho^{(f)}C)/(HM - C^2) + k^2}{\gamma_{Ps}^2 - \gamma_{Pf}^2}, \tag{54}$$

$$\breve{K}_{SS}^{mff} = \hat{L} \frac{s^2\rho/G^{(fr)} + k^2}{\gamma_{EM}^2 - \gamma_S^2}, \tag{55}$$

$$\breve{K}_{SS}^{\tau ff} = \frac{\rho^{(f)}}{\rho^{(E)}} \frac{\zeta\varsigma + k^2}{\gamma_{EM}^2 - \gamma_S^2}, \tag{56}$$

$$\breve{K}_{PP}^{\tau ff} = -2\left(\frac{G^{(fr)}C}{HM - C^2}\right) \frac{s^2\rho^{(f)}/C + k^2}{\gamma_{Ps}^2 - \gamma_{Pf}^2}, \tag{57}$$

$$\breve{N}_{PP}^{\tau ff} = -\left(\frac{1}{HM - C^2}\right) \frac{s^2(\rho^{(f)}H - \rho C)}{\gamma_{Ps}^2 - \gamma_{Pf}^2}. \tag{58}$$

The coefficients for the fields generated by the volume injection rate source, which cannot be directly found from reciprocity, are given by

$$\breve{K}_{PP}^{pq} = \frac{s\rho\eta^{(e)}}{\varsigma} \frac{s^2(\rho - (\rho^{(f)})^2\varsigma/(\rho^{(E)}\eta^{(e)}))M/(HM - C^2) + k^2}{\gamma_{Ps}^2 - \gamma_{Pf}^2}, \tag{59}$$

$$\breve{K}_{PP}^{\tau q} = -2\left(\frac{2G^{(fr)}}{HM - C^2}\right) \frac{s(\rho^{(E)}\eta^{(e)}C/\varsigma - \rho^{(f)}M)}{\gamma_{Ps}^2 - \gamma_{Pf}^2}, \tag{60}$$

$$\breve{N}_{PP}^{\tau q} = s\rho^{(f)} \frac{s^2C(\rho\rho^{(E)}\eta^{(e)}/(\rho^{(f)}\varsigma) - \rho^{(f)})/(HM - C^2) + k^2}{\gamma_{Ps}^2 - \gamma_{Pf}^2}. \tag{61}$$

The coefficients for the fields generated by a magnetic current source, which cannot be directly found from reciprocity, are given by

$$\breve{K}_{SS}^{mm} = \frac{s^2\rho^{(c)} + k^2}{\gamma_{EM}^2 - \gamma_S^2}, \tag{62}$$

$$\breve{N}_{SS}^{mm} = -\frac{(s\rho^{(f)}\hat{L})^2 s/G^{(fr)}}{\gamma_{EM}^2 - \gamma_S^2}, \tag{63}$$

$$\breve{K}_{SS}^{\tau m} = \frac{s\rho^{(f)}\hat{L}}{\gamma_{EM}^2 - \gamma_S^2}. \tag{64}$$

The coefficients for the stress field generated by a deformation rate source, which cannot be directly found from reciprocity, are given by

$$\breve{K}^{\tau h}_{SS} = \frac{G^{(fr)}(\zeta\eta^{(e)} + k^2)}{s(\gamma^2_{EM} - \gamma^2_S)}, \tag{65}$$

$$\breve{K}^{\tau h}_{PP} = 2\frac{G^{(fr)}}{s}\frac{k^4 + k^2s^2(\rho^{(E)}H\eta^{(e)}/\varsigma - \rho^{(f)}C)/(HM - C^2)}{\gamma^2_{Ps} - \gamma^2_{Pf}}, \tag{66}$$

$$\breve{N}^{\tau h}_{PP} = \frac{Hk^4 + k^2s^2(\rho^{(E)}H^2\eta^{(e)}/\varsigma - 2\rho^{(f)}HC + \rho C^2)/(HM - C^2)}{s(\gamma^2_{Ps} - \gamma^2_{Pf})}, \tag{67}$$

$$\breve{Q}^{\tau h}_{Pf} = \left(\frac{4(G^{(fr)})^2}{s(HM - C^2)}\right)\frac{Mk^4 + k^2s^2\rho^{(E)}\eta^{(e)}/\varsigma}{\gamma^2_{Ps} - \gamma^2_{Pf}}. \tag{68}$$

With these coefficients all Green's functions are defined in the wavenumber-frequency domain. In the numerical codes provided with this paper all these Green's functions are computed and used in the basic equations to verify correctness numerically. The results are not shown in the paper, but can be obtained by running the codes available in the folder for wavenumber-frequency domain modeling where one script file for each source type is availabe to run the test. In the next section the space-frequency domain Green's functions are given.

SPACE-DOMAIN GREEN'S FUNCTIONS

Inverse spatial Fourier transformation as outlined in Appendix C gives the space-frequency domain Green's functions. We use the scalar and six tensor Green's functions for the four separate wave types derived in Appendix C to write the results. The Green's functions are given by

$$\hat{G}^{rs}_{ij}(\boldsymbol{x}, s) = \hat{K}^{rs}_S\hat{G}^S_{ij}(\boldsymbol{x}, s) - \hat{K}^{rs}_{EM}\hat{G}^{EM}_{ij}(\boldsymbol{x}, s) + \hat{K}^{rs}_{Pf}\hat{\mathcal{G}}^{Pf}_{ij}(\boldsymbol{x}, s) - \hat{K}^{rs}_{Ps}\hat{\mathcal{G}}^{Ps}_{ij}(\boldsymbol{x}, s), \tag{69}$$

$$\hat{G}^{ps}_{i}(\boldsymbol{x}, s) = \hat{K}^{ps}_{Pf}\hat{G}^{Pf}_{i}(\boldsymbol{x}, s) - \hat{K}^{ps}_{Pf}\hat{G}^{Ps}_{i}(\boldsymbol{x}, s), \tag{70}$$

$$\hat{G}^{ms}_{ij}(\boldsymbol{x}, s) = \epsilon_{imj}\left(\hat{K}^{ms}_S\hat{G}^S_m(\boldsymbol{x}, s) - \hat{K}^{ms}_{EM}\hat{G}^{EM}_m(\boldsymbol{x}, s)\right). \tag{71}$$

$$\begin{aligned}\hat{G}^{\tau s}_{ijk}(\boldsymbol{x}, s) = {}& \hat{K}^{\tau s}_S\left(\hat{G}^S_{ikj}(\boldsymbol{x}, s) + \hat{G}^S_{jki}(\boldsymbol{x}, s)\right) - \hat{K}^{\tau s}_{EM}\left(\hat{G}^{EM}_{ikj}(\boldsymbol{x}, s) + \hat{G}^{EM}_{jki}(\boldsymbol{x}, s)\right)\\ &+\hat{K}^{\tau s}_{Pf}\hat{G}^{Pf}_{ijk}(\boldsymbol{x}, s) - \hat{K}^{\tau s}_{Ps}\hat{G}^{Ps}_{ijk}(\boldsymbol{x}, s) + \left(\hat{N}^{\tau s}_{Pf}\hat{G}^{Pf}_{k}(\boldsymbol{x}, s) - \hat{N}^{\tau s}_{Ps}\hat{G}^{Ps}_{k}(\boldsymbol{x}, s)\right)\delta_{ij},\end{aligned} \tag{72}$$

$$\hat{G}^{pq}(\boldsymbol{x}, s) = \hat{K}^{pq}_{Pf}\hat{G}^{Pf}(\boldsymbol{x}, s) - \hat{K}^{pq}_{Ps}\hat{G}^{Ps}(\boldsymbol{x}, s), \tag{73}$$

$$\hat{G}^{mq}_{i}(\boldsymbol{x}, s) = \hat{G}^{pm}_{i}(\boldsymbol{x}, s) = 0, \tag{74}$$

$$\hat{G}^{\tau q}_{ij}(\boldsymbol{x}, s) = \hat{K}^{\tau q}\left(\gamma^2_{Pf}\hat{G}^{Pf}_{ij}(\boldsymbol{x}, s) - \gamma^2_{Ps}\hat{G}^{Ps}_{ij}(\boldsymbol{x}, s)\right) + (\hat{N}^{\tau q}_{Pf}\hat{G}^{Pf}(\boldsymbol{x}, s) - \hat{N}^{\tau q}_{Ps}\hat{G}^{Ps}(\boldsymbol{x}, s))\delta_{ij}, \tag{75}$$

$$\begin{aligned}\hat{G}^{mm}_{ij}(\boldsymbol{x}, s) = {}& \hat{K}^{mm}_S\left(\gamma^2_S\zeta^{-1}\hat{\mathcal{G}}^S_{ij}(\boldsymbol{x}, s) - \eta^{(e)}\hat{G}^S(\boldsymbol{x}, s)\delta_{ij}\right) - \hat{N}^{mm}\hat{G}^S(\boldsymbol{x}, s)\delta_{ij}\\ &-\hat{K}^{mm}_{EM}\left(\gamma^2_{EM}\zeta^{-1}\hat{\mathcal{G}}^{EM}_{ij}(\boldsymbol{x}, s) - \eta^{(e)}\hat{G}^{EM}(\boldsymbol{x}, s)\delta_{ij}\right) + \hat{N}^{mm}\hat{G}^{EM}(\boldsymbol{x}, s)\delta_{ij},\end{aligned} \tag{76}$$

$$\begin{aligned}\hat{G}^{\tau m}_{ijk}(\boldsymbol{x}, s) = {}& \hat{K}^{\tau m}\left(\gamma^2_S\left(\epsilon_{imk}\hat{\mathcal{G}}^S_{mj}(\boldsymbol{x}, s) + \epsilon_{jmk}\hat{\mathcal{G}}^S_{mi}(\boldsymbol{x}, s)\right)\right.\\ &\left.-\gamma^2_{EM}\left(\epsilon_{imk}\hat{\mathcal{G}}^{EM}_{mj}(\boldsymbol{x}, s) + \epsilon_{jmk}\hat{\mathcal{G}}^{EM}_{mi}(\boldsymbol{x}, s)\right)\right),\end{aligned} \tag{77}$$

$$\begin{aligned}\hat{G}^{\tau h}_{ijkl}(\boldsymbol{x},s) &= \hat{K}^{\tau h}_{Pf}\left(\delta_{ij}\hat{G}^{Pf}_{kl}(\boldsymbol{x},s)+\hat{G}^{Pf}_{ij}(\boldsymbol{x},s)\delta_{kl}\right)+\hat{Q}^{\tau h}_{Pf}\hat{G}^{Pf}_{ijkl}(\boldsymbol{x},s)\\
&-\hat{K}^{\tau h}_{Ps}\left(\delta_{ij}\hat{G}^{Ps}_{kl}(\boldsymbol{x},s)+\hat{G}^{Ps}_{ij}(\boldsymbol{x},s)\delta_{kl}\right)-\hat{Q}^{\tau h}_{Ps}\hat{G}^{Ps}_{ijkl}(\boldsymbol{x},s)\\
&+\hat{N}^{\tau h}_{Pf}\hat{G}^{Pf}(\boldsymbol{x},s)\delta_{ij}\delta_{kl}-\hat{N}^{\tau h}_{Ps}\hat{G}^{Ps}(\boldsymbol{x},s)\delta_{ij}\delta_{kl}\\
&+\hat{K}^{\tau h}_{S}\left(\hat{\mathcal{G}}^{S}_{ikjl}(\boldsymbol{x},s)+\hat{\mathcal{G}}^{S}_{iljk}(\boldsymbol{x},s)+\hat{\mathcal{G}}^{S}_{jkil}(\boldsymbol{x},s)+\hat{\mathcal{G}}^{S}_{jlik}(\boldsymbol{x},s)\right)\\
&-\hat{K}^{\tau h}_{EM}\left(\hat{\mathcal{G}}^{EM}_{ikjl}(\boldsymbol{x},s)+\hat{\mathcal{G}}^{EM}_{iljk}(\boldsymbol{x},s)+\hat{\mathcal{G}}^{EM}_{jkil}(\boldsymbol{x},s)+\hat{\mathcal{G}}^{EM}_{jlik}(\boldsymbol{x},s)\right)\\
&-\left((H-2G^{(fr)})\delta_{ij}\delta_{kl}-G^{(fr)}(\delta_{ik}\delta_{jl}+\delta_{il}\delta_{jk})\right)\frac{\delta(\boldsymbol{x})}{s}.\end{aligned}\tag{78}$$

The field coefficients for any source type are equal to the wavenumber domain coefficients with substitution of $k=\mathrm{i}\gamma_W$ for each wave type to which the coefficient belongs, as shown in Appendix C. As an example the S-wave and Pf-wave coefficients for the particle velocity generated by a force source acting on the bulk are given by

$$\hat{K}^{vf}_{S}=\check{K}^{vf}_{SS}(k=\mathrm{i}\gamma_S),\tag{79}$$

$$\hat{K}^{vf}_{Pf}=\check{K}^{vf}_{PP}(k=\mathrm{i}\gamma_{Pf}).\tag{80}$$

All other coefficients can be found in the same way. Similarly source-receiver reciprocity relations in space-domain can be directly obtained from the wavenumber domain counterparts, e.g.,

$$\hat{G}^{vq}_{ij}(\boldsymbol{x},\boldsymbol{x}^s,s)=-\hat{G}^{pf}_{ji}(\boldsymbol{x}^s,\boldsymbol{x},s),\tag{81}$$

$$\hat{G}^{vh}_{ijk}(\boldsymbol{x},\boldsymbol{x}^s,s)=\hat{G}^{\tau f}_{kji}(\boldsymbol{x}^s,\boldsymbol{x},s),\tag{82}$$

where it is noted that in the latter example not only source-receiver subscripts are interchanged, but also the two subscripts related to the deformation rate source are interchanged when related to the stress field. The other relations can be found in a similar way.

NUMERICAL RESULTS

The code that is available with the paper computes all fields generated by each type of source and will do so very fast on a simple desktop computer. However, to avoid a large number of figures here we show a limited number of field responses. Because the coupling coefficient is small, converted wavefields are small for seismic fields generated by seismic sources and for electromagnetic fields from electromagnetic sources. We therefore concentrate on seismic fields generated by electromagnetic sources. Because the magnetic current source only creates transversal waves it is sufficient to look at the seismic field responses to an electric current source. The reverse fields can be understood from source-receiver reciprocity. In this section we use x for x_1, y for x_2 and z for x_3. We take an electric current source in the origin and a grid of receivers in the (x,y)-plane at some depth below the source. The time source signature is a Ricker wavelet with center frequency of 40 Hz and of 400 kHz to mimic field seismic and ultrasonic measurement regimes. The medium parameters that have been used to generate the results are given in Table 1.

We compute the particle velocity and filtration velocity fields generated by an electric current source emitting a Ricker wavelet with center frequency of 40 Hz in the horizontal

plane at a depth of $z = 50$ m below the source location. We show the four different wave types separately for $G^{ve}_{11}(x, y, z, t)$ in Figure 1 and $G^{we}_{11}(x, y, z, t)$ in Figure 2 for fixed z and $t = 98$ ms. The first observation is that in a single field the amplitudes of the four wave types differ by more than 10 orders of magnitude. The propagating waves are the S-wave and the fast P-wave and their amplitude difference four orders of magnitude.The S-waves shown in Figures 1a and 2a have a maximum propagation amplitude in the y-direction. It can be seen that the particle velocity S-wave is more than three orders of magnitude stronger than that of the filtration velocity. The particle velocity and filtration velocity in the electromagnetic and the slow P-waves of these fields are diffusive fields in the frequency band of the Ricker wavelet as can be seen from Figures 1b, 2b and 1c, 2c, respectively. In this snapshot their amplitudes are several orders of magnitude smaller than those of the propagating waves. The reason for the low amplitude of the particle velocity in the electromagnetic field is because the signal essentially arrives at $t = 0$ and there it has a maximum amplitude that is on the order of 10^{-12} and the signal has a short duration of the time window of the Ricker wavelet. Hence, the particle velocity in the electromagnetic field has a similar maximum amplitude as the fast P-wave. For the slow P-wave it is different because the diffusion process is very slow and the signal is spread out over the whole time window, but with extremely small amplitude. The fast P-waves are shown in Figures 1d and 2d. They propagate with maximum amplitude in the x-direction and the particle velocity fast P-wave is more than three orders of magnitude stronger than that of the filtration velocity. The ratio of maximum amplitude of fast P-wave and S-wave in the particle velocity and the filtration velocity fields is approximately 5×10^3. We can also observe that the particle velocity and filtration velocity fields have opposite polarity. The stress-field is similar, but because it has one extra gradient the radiation pattern is slightly different and is not shown here.

We compute the particle velocity and filtration velocity fields generated by an electric current source emitting a Ricker wavelet with center frequency of 400 kHz in the horizontal plane at a depth of $z = 5$ mm below the source location. At these frequencies we cannot use the static values for the permeability and coupling coefficients and we use the following relations

$$\hat{k}(\omega) = k_0 \left(\sqrt{1 + sm/(2\omega_c)} + s/(\omega_c) \right)^{-1}, \tag{83}$$

$$\hat{L}(\omega) = L_0 \left(1 + 2s/(m\omega_c)\right)^{-1/2}, \tag{84}$$

in which m is a shape factor that we take as $m = 8$ and ω_c is the critical frequency given by $\omega_c = \phi\eta/(\alpha_\infty k_0 \rho^{(f)})$ and in our example $\omega_c = 76.9$ kHz. We show the four different wave types separately for $G^{ve}_{11}(x, y, z, t)$ in Figure 3a-3d and $G^{we}_{11}(x, y, z, t)$ in Figure 4a-4d for fixed $z = 5$ mm and $t = 9.8$ μs. The shear-waves can be seen in Figures 3a and 4a and it can be seen that the particle velocity S-wave is an order of magnitude stronger than that of the filtration velocity. The particle velocity and filtration velocity in the electromagnetic field is still diffusive in the ultrasonic frequency band of the Ricker wavelet as can be seen from Figures 3b and 4b. The reason for the low amplitude of the particle velocity in the electromagnetic field is because the signal essentially arrives at $t = 0$ and there it has a maximum amplitude and the signal has a short duration of the time window of the Ricker wavelet so we observe the tail end of the Ricker wavelet. At these frequencies the slow P-wave is a propagating wave with a propagation velocity below that of the shear wave as can be seen in Figures 3c and 4c, respectively. The slow P-waves are the strongest signal

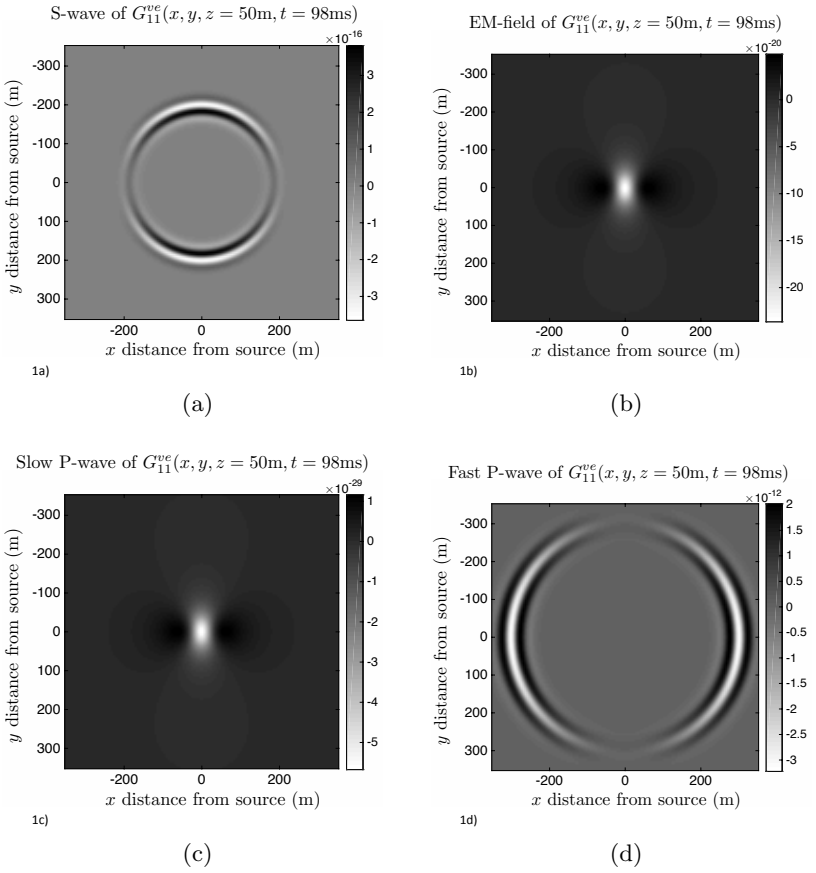

Figure 1: The particle velocity response to an electric current source; S-wave (a), EM-field (b), Ps-field (c), and Pf-wave (d).

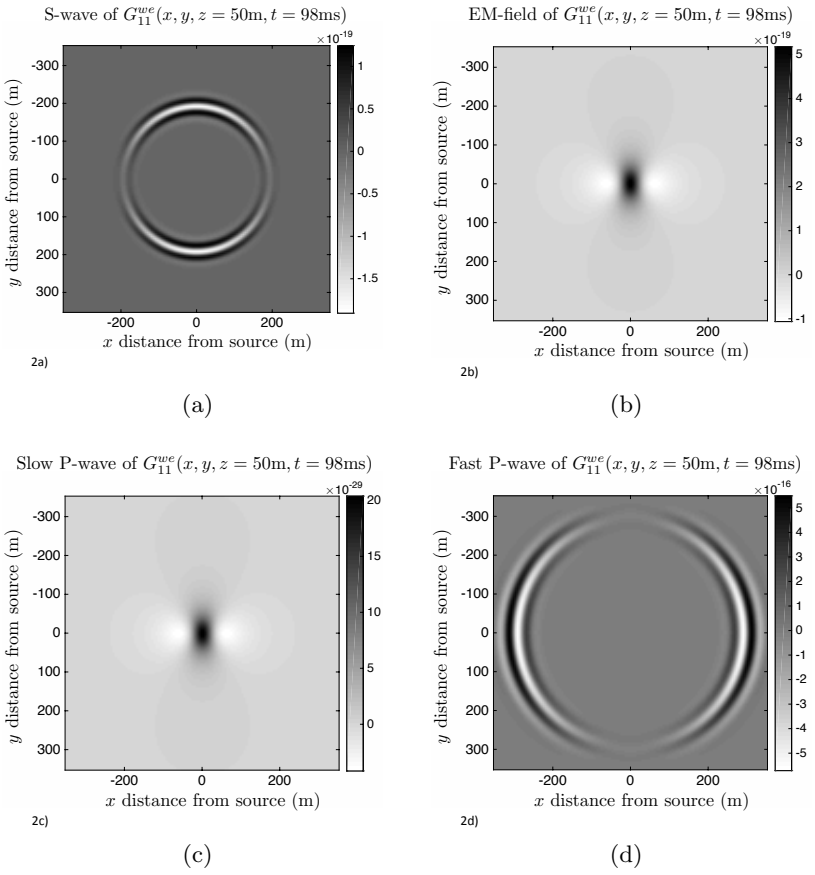

Figure 2: The filtration velocity response to an electric current source; S-wave (a), EM-field (b), Ps-field (c), and Pf-wave (d).

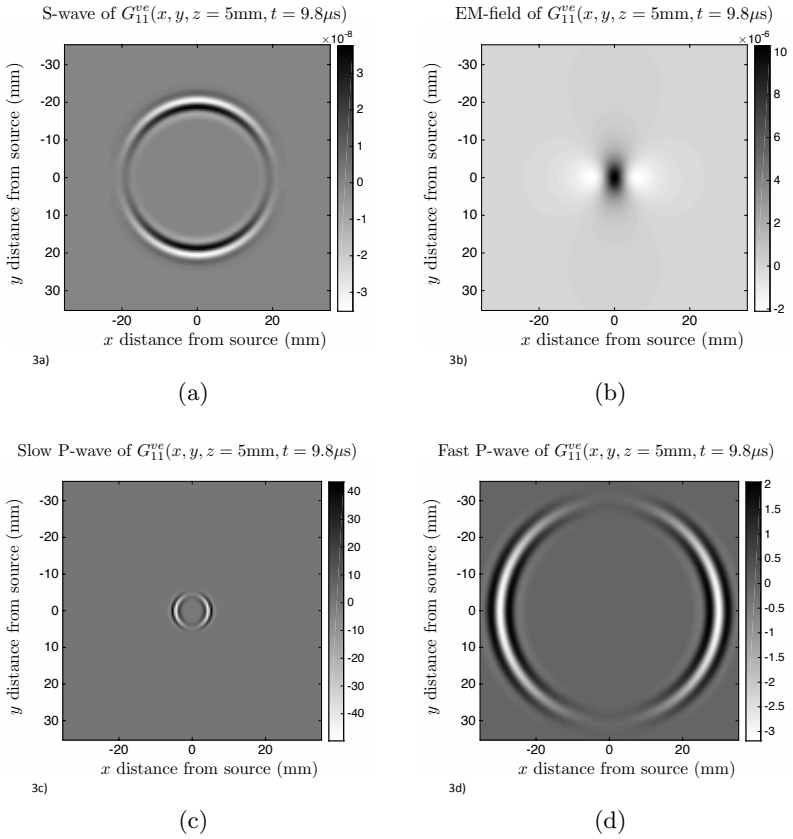

Figure 3: The ultrasonic particle velocity response to an electric current source; S-wave (a), EM-field (b), Ps-field (c), and Pf-wave (d).

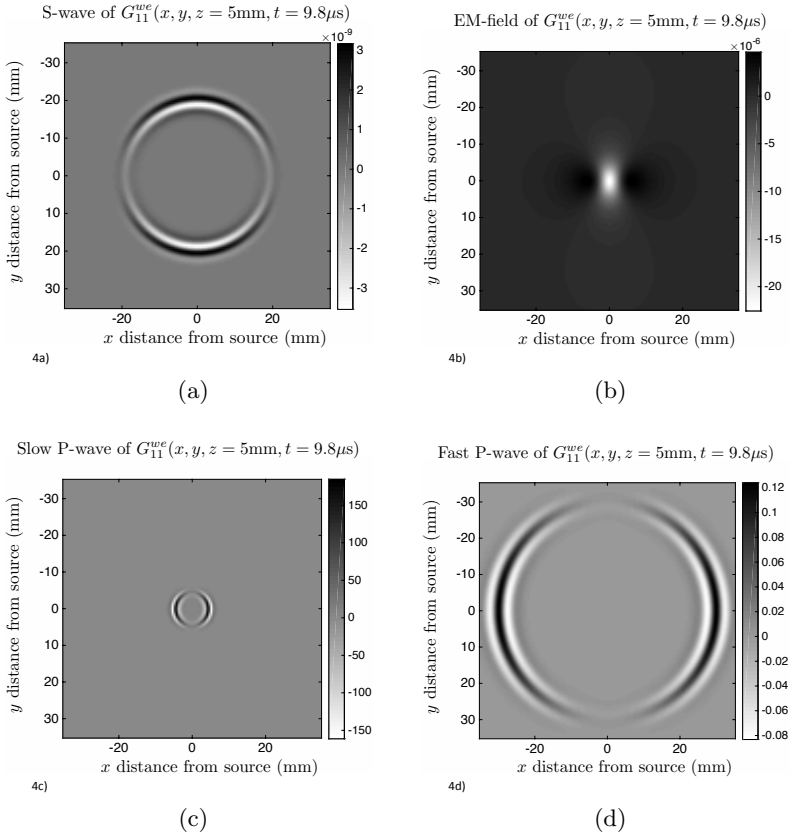

Figure 4: The ultrasonic filtration velocity response to an electric current source; S-wave (a), EM-field (b), Ps-field (c), and Pf-wave (d).

in this frequency band and the filtration velocity slow P-wave is more than three times stronger than that of the particle velocity. The fast P-waves are shown in Figures 1d and 2d and the particle velocity fast P-wave is just over one order of magnitude stronger than that of the filtration velocity. The ratio of maximum amplitude of fast P-wave and S-wave in the particle velocity and the filtration velocity fields has increased compared to the low frequency example above to approximately 10^8. We can observe that the particle velocity and filtration velocity fields have opposite polarity. We can also observe that the electric field at seismic frequencies has opposite polarity relative to the electric field at ultrasonic frequencies.

CONCLUSIONS

We have derived closed-form expressions for the Green's functions corresponding to all fields and any type of source. This was done by reducing the coupled system of equations to an algebraic system for the particle velocity and the electric field in the wavenumber-frequency domain. The solution of this reduced set naturally leads to separated solutions for transversal and longitudinal wavefields and is given in terms of four tensors of rank two. These tensors are the time-step response Green's functions for the particle velocity and electric field generated by a force source acting on the bulk and the fluid, respectively. All Green's functions for the particle velocity generated by other sources are linear combinations of the Green's functions for the particle velocity generated by a force source acting on the bulk and the fluid. Similarly, all Green's functions for the electric field generated by other sources are linear combinations of the Green's functions for the electric field generated by a force source acting on the bulk and the fluid. From these expressions and the basic equations the Green's functions for all fields generated by any source can be found algebraically. After these are found a three-dimensional inverse spatial Fourier transformation could be evaluated analytically to find closed-form expression for all the Green's functions in space-frequency domain. Space-time domain results are then obtained numerically using an inverse FFT routine.

We have provided numerical codes in which all fields are computed for a particular source and substituted the results in the basic equations in wavenumber-frequency domain to demonstrate correctness of the results. This is done for all sources, but for a single component, which suffices to demonstrate correctness of the obtained results. We have also provided numerical codes to compute all fields generated by each source separately. For an electric current source we have shown numerical results by separating the four wave types. This allowed to analyse and compare the results. At seismic frequencies the fast P-wave is radiated with the strongest amplitude in all fields, except for the magnetic field where only transversal waves are generated. At ultrasonic frequencies the slow P-wave is the strongest signal of the four types. In the filtration and particle velocity fields generated by an electric current source the slow P-wave is, respectively, three orders and one order of magnitiude lager than the fast P-wave, which is the second strongest wave component in these fields.

REFERENCES

Bordes, C., L. Jouniaux, M. Dietrich, J.-P. Pozzi, and S. Garambois, 2006, First laboratory measurements of seismo-magnetic conversions in fluid-filled fontainebleau sand:

Geophysical Research Letters, **33**, L01302.

Bordes, C., L. Jouniaux, S. Garambois, M. Dietrich, J.-P. Pozzi, and S. Gaffet, 2008, Evidence of the theoretically predicted seismo-magnetic conversion: Geophysical Journal International, **174**, 489–504.

Bordes, C., P. Sénéchal, J. Barrière, D. Brito, E. Normandin, and D. Jougnot, 2015, Impact of water saturation on seismoelectric transfer functions: a laboratory study of coseismic phenomenon: Geophysical Journal International, **200**, 1317–1355.

Butler, K. E., R. D. Russel, A. W. Kepic, and M. Maxwell, 1996, Measurement of the seismoelectric response from a shallow boundary: Geophysics, **61**, 1769–1778.

Gao, Y., and H. Hu, 2010, Seismoelectromagnetic waves radiated by a double couple source in a saturated porous medium: Geophysical Journal International, **181**, 873–896.

Garambois, S., and M. Dietrich, 2001, Seismoelectric wave conversions in porous media: Field measurements and transfer function analysis: Geophysics, **66**, 1417–1430.

———, 2002, Full waveform numerical simulations of seismoelectromagnetic wave conversions in fluid-saturated stratified porous media: Journal of Geophysical Research-Solid Earth, **107**, B72148.

Guan, W., H. S. Hu, and X. B. Zheng, 2013, Theoretical simulation of the multipole seismoelectric logging while drilling: Geophysical Journal International, **195**, 1239–1250.

Haartsen, M. W., and S. R. Pride, 1997, Electroseimic waves from point sources in layered media: Journal of Geophysical Research - Solid Earth, **102**, 24745–24769.

Haartsen, M. W., W. Dong and M. N. Toks oz, 1998, Dynamic streaming currents from seismic point sources in homogeneous poroelastic media: Geophysical Journal International, **132**, 256-274.

Haas, A., A. Revil, M. Karoulis, L. Frash, J. Hampton, M. Gutierrez, and M. Mooney, 2013, Waveform joint inversion of seismograms and electrograms for moment tensor characterization of fracking events: Geophysics, **78**, no. 2, D93–D113.

Haines, S. S., and S. R. Pride, 2006, Seismoelectric modeling on a grid: Geophysics, **71**, no. 6, N57–N65.

Haines, S. S., S. R. Pride, S. L. Klemperer, and B. Biondi, 2007, Seismoelectric imaging of shallow targets: Geophysics, **72**, no. 2, G9–G20.

Han, Q., and Z. Wang, 2001, Time-domain simulation of SH-wave induced electromagnetic field in heterogeneous porous media: A fast finite-element algorithm: Geophysics, **66**, 448–461.

Hu, H., and Y. Gao, 2011, Electromagnetic field generated by a finite fault due to electrokinetic effect: Journal of Geophysical Research, **116**, B08302.

Ivanov, A. G., 1940, Seismoelectric effect of the second kind (in russian): Bulletin Academy of Sciences USSR, série géographique et géophysique, **5**, 699–727.

Jardani, A., and A. Revil, 2015, Seismoelectric couplings in a poroelastic material containing two immiscible fluid phases: Geophysical Journal International, **202**, 850–870.

Karakelian, D., G. C. Beroza, S. L. Klemperer, and A. C. Frazer-Smith, 2002, Analysis of ultralow-frequency electromagnetic field measurements associated with the 1999 M7.1 Hector Mine, California, Earthquake Sequence: Bulletin of the Seismological Society of America, **92**, 1513–1524.

Karpfinger, F., T. M. Müller, and B. Gurevich, 2009, Green's functions and radiation patterns in poroelastic solids revisited: Geophysical Journal International, **178**, 327–337.

Kepic, A. W., M. Maxwell, and R. D. Russell, 1995, Field trials of a seismoelectric method for detecting massive sulfides: Geophysics, **60**, 365–373.

Kroeger, B., U. Yaramanci, and A. Kemna, 2014, Numerical analysis of seismoelectric wave

propagation in spatially confined geological units: Geophysical Prospecting, **62**, 133–147.
Mahardika, H., A. Revil, and A. Jardani, 2012, Waveform joint inversion of seismograms and electrograms for moment tensor characterization of fracking events: Geophysics, **77**, no. 5, ID23–ID29.
Martner, S. T., and N. R. Sparks, 1959, The electroseismic effect: Geophysics, **14**, 279–308.
Mikhailov, O. V., J. Queenz, and M. N. Toksöz, 2000, Using borehole electroseismic measurements to detect and characterize fractured (permeable) zones: Geophysics, **65**, 1098–1112.
Pride, S. R., 1994, Governing equations for the coupled electromagnetics and acoustics of porous media: Physical Review B, **50**, 678–696.
Pride, S. R., and M. W. Haartsen, 1996, Electroseimic wave properties: Journal of the Acoustical Society of America, **100**, 1301–1315.
Ren, H., Q. Huang, and X. Chen, 2010, A new numerical technique for simulating the coupled seismic and electromagnetic waves in layered porous media: Earthquake Science, **23**, 167–176.
Revil, A., and H. Mahardika, 2013, Coupled hydromechanical and electromagnetic disturbances in unsaturated porous materials: Water Resources Research, **49**, 744–766.
Schakel, M. D., D. M. J. Smeulders, E. C. Slob, and H. K. J. Heller, 2011a, Laboratory measurements and theoretical modeling of seismoelectric interface response and coseismic wave fields: Journal of Applied Physics, **109**.
———, 2011b, Seismoelectric interface response: Experimental results and forward model: Geophysics, **76**, no. 4, N29–N36.
Schoemaker, F., N. Grobbe, M. D. Schakel, S. A. L. de Ridder, E. C. Slob, and D. M. J. Smeulders, 2012, Experimental validation of the electrokinetic theory and development of seismoelectric interferometry by cross-correlation: International Journal of Geophysics, **2012**, 514242.
Thompson, A. H., S. Hornbostel, T. M. J. Burns, R. Raschke, J. Wride, P. McCammon, J. Sumner, G. Haake, M. Bixby, W. Ross, B. S. White, M. Zhou, and P. Peczak, 2007, Field tests of electroseismic hydrocarbon detection: Geophysics, **72**, no. 1, N1–N9.
Thompson, R. R., 1936, The seismic electric effect: Geophysics, **1**, 327–335.
Warden, S., S. Garambois, P. Sailhac, L. Jouniaux, and M. Bano, 2012, Curvelet-based seismoelectric data processing: Geophysical Journal International, **190**, 1533–1550.
Zhu, Z., M. W. Haartsen, and M. N. Toksöz, 1999, Experimental studies of electrokinetic conversions in fluid-saturated borehole models: Geophysics, **64**, 1349–1356.
Zhu, Z., and M. N. Toksöz, 2005, Seismoelectric and seismomagnetic measurements in fractured borehole models: Geophysics, **70**, no. 4, F45–F51.
Zhu, Z., M. N. Toksöz, and D. Burns, 2008, Electroseismic and seismoelectric measurements of rock samples in a water tank: Geophysics, **73**, no. 5, E153–E164.
Zyserman, F. I., P. M. Gauzellino, and J. E. Santos, 2010, Finite element modeling of SHTE and PSVTM electroseismics: Jounral of Applied Geophysics, **72**, 79–91.

APPENDIX A: REDUCTION TO COUPLED EQUATIONS FOR ELECTRIC FIELD AND PARTICLE VELOCITY

Here we reduce the system of equations to coupled equations for the electric field and the particle velocity, by eliminating all other fields. We start by eliminating $\hat{H}_j$ from equation 3

with the aid of equation 4, which gives

$$-k_k k_m \breve{E}_m + k^2 \breve{E}_k + \zeta\varsigma \breve{E}_k + s\zeta\rho^{(E)}\hat{L}\breve{w}_k = -\zeta \breve{J}^{(e)}_k + \epsilon_{kmp}\mathrm{i}k_m \breve{J}^{(m)}_p, \tag{A-1}$$

in which $k^2 = k_m k_m$. Equation A-1 relates the electric field and the filtration velocity to the action of electric and magnetic current sources. By taking the scalar product with $\boldsymbol{k}$ in equation A-1 we obtain

$$\varsigma k_m \breve{E}_m + s\rho^{(E)}\hat{L}k_n\breve{w}_n = -k_r \breve{J}^{(e)}_r, \tag{A-2}$$

which allows expressing $k_n\breve{w}_n$ in terms of $k_n\breve{E}_n$ and $k_n\breve{J}^{(e)}_n$. We now eliminate $\breve{p}$ using equation 10 in equation 8 and find

$$\begin{aligned} s^2\rho^{(f)}\breve{v}_i + Ck_ik_m\breve{v}_m + s^2\rho^E(\breve{w}_i - \hat{L}\breve{E}_i) + Mk_ik_m\breve{w}_m = \\ s\breve{f}^{(f)}_i + C\mathrm{i}k_i\breve{h}_{mm} + M\mathrm{i}k_i\breve{q}, \end{aligned} \tag{A-3}$$

from which we eliminate $\breve{w}_i$ and $k_m\breve{w}_m$ using equations A-1 and A-2 yielding

$$\begin{aligned} &s^2\rho^{(f)}\breve{v}_k + Ck_kk_m\breve{v}_m - \frac{s}{\hat{L}\zeta}(k^2 + \eta^{(e)}\zeta)\breve{E}_k + \left(\frac{s}{\hat{L}\zeta} - \frac{M\varsigma}{s\rho^{(E)}\hat{L}}\right)k_kk_m\breve{E}_m \\ &= s\breve{f}^{(f)}_k + (C\breve{h}_{mm} + M\breve{q})\mathrm{i}k_k + \frac{s}{\hat{L}}\left(\breve{J}^{(e)}_k - \zeta^{-1}\epsilon_{kmp}\mathrm{i}k_m\breve{J}^{(m)}_p\right) + \frac{M}{s\rho^{(E)}\hat{L}}k_kk_n\breve{J}^{(e)}_n. \end{aligned} \tag{A-4}$$

Equation A-4 is the first equation that we need to find Green's function expressions for the electric field and particle velocity.

For the second set of equations we start by eliminating $\breve{\tau}_{ij}$ from equation 7 using equation 9, which leads to

$$s^2\rho\breve{v}_i + c_{ijkl}k_jk_l\breve{v}_k + s^2\rho^{(f)}\breve{w}_i + Ck_ik_m\breve{w}_m = c_{ijkl}\mathrm{i}k_j\breve{h}_{kl} + C\mathrm{i}k_i\breve{q} + s\breve{f}_i, \tag{A-5}$$

from which we eliminate $\breve{w}_i$ and $k_m\breve{w}_m$ using equations A-1 and A-2 resulting in

$$\begin{aligned} &s^2\rho\breve{v}_i + c_{ijkl}k_jk_l\breve{v}_k - \frac{s\rho^{(f)}}{\rho^{(E)}\hat{L}\zeta}(k^2 + \zeta\varsigma)\breve{E}_i + \left(\frac{s\rho^{(f)}}{\rho^{(E)}\hat{L}\zeta} - \frac{C\varsigma}{s\rho^{(E)}\hat{L}}\right)k_ik_m\breve{E}_m \\ &= s\breve{f}_i + c_{ijkl}\mathrm{i}k_j\breve{h}_{kl} + C\mathrm{i}k_i\breve{q} + \frac{s\rho^{(f)}}{\rho^{(E)}\hat{L}}\left(\breve{J}^{(e)}_i - \zeta^{-1}\epsilon_{imp}\mathrm{i}k_m\breve{J}^{(m)}_p\right) + \frac{C}{s\rho^{(E)}\hat{L}}k_ik_n\breve{J}^{(e)}_n. \end{aligned} \tag{A-6}$$

We substitute the expression for c_{ijkl} of equation 11 in equation A-6 to obtain an expression where the particle velocity and its divergence occur explicitly

$$\begin{aligned} &\left(G^{(fr)}k^2 + s^2\rho\right)\breve{v}_i + \left(H - G^{(fr)}\right)k_ik_m\breve{v}_m - \frac{s\rho^{(f)}}{\rho^{(E)}\hat{L}\zeta}(k^2 + \varsigma\zeta)\breve{E}_i - \frac{C\varsigma\zeta - s^2\rho^{(f)}}{s\rho^{(E)}\hat{L}\zeta}k_ik_m\breve{E}_m \\ &\qquad = s\breve{f}_i + \left(H - 2G^{(fr)}\right)\mathrm{i}k_i\breve{h}_{kk} + 2G^{(fr)}\mathrm{i}k_j\breve{h}_{ij} + C\mathrm{i}k_i\breve{q} \\ &\qquad + \frac{s\rho^{(f)}}{\rho^{(E)}\hat{L}}\left(\breve{J}^{(e)}_i - \zeta^{-1}\epsilon_{imp}\mathrm{i}k_m\breve{J}^{(m)}_p\right) + \frac{C}{s\rho^{(E)}\hat{L}}k_ik_n\breve{J}^{(e)}_n. \end{aligned} \tag{A-7}$$

with $H = K_G + 4G^{(fr)}/3$. Equation A-7 is the second equation for the electric field and the particle velocity. Equations A-4 and A-7 can be combined in a matrix equation given by

$$\begin{pmatrix} a_{11}\delta_{ij} + b_{11}k_ik_j & a_{12}\delta_{ik} + b_{12}k_ik_k \\ a_{21}\delta_{pj} + b_{21}k_pk_j & a_{22}\delta_{pk} + b_{22}k_pk_k \end{pmatrix}\begin{pmatrix} \breve{v}_j \\ \breve{E}_k \end{pmatrix} = \begin{pmatrix} \breve{F}_{i;1} \\ \breve{F}_{p;2} \end{pmatrix}, \tag{A-8}$$

with the source vectors given by

$$\begin{pmatrix} \breve{F}_{i;1} \\ \breve{F}_{p;2} \end{pmatrix} = \begin{pmatrix} s\breve{f}_i^{(f)} + C\mathrm{i}k_i\breve{h}_{mm} + M\mathrm{i}k_i\breve{q} \\ s\breve{f}_p + (H-2G^{(fr)})\mathrm{i}k_p\breve{h}_{mm} + 2G^{(fr)}\mathrm{i}k_j\breve{h}_{pj} + C\mathrm{i}k_p\breve{q} \end{pmatrix} + \begin{pmatrix} \left(\frac{s}{\hat{L}}\delta_{ij} + \frac{M}{s\rho^{(E)}\hat{L}}k_ik_j\right)\breve{J}_j^{(e)} - \frac{s}{\hat{L}\zeta}\epsilon_{ijk}\mathrm{i}k_j\breve{J}_k^{(m)} \\ \left(\frac{s\rho^{(f)}}{\rho^{(E)}\hat{L}}\delta_{pq} + \frac{C}{s\rho^{(E)}\hat{L}}k_pk_q\right)\breve{J}_q^{(e)} - \frac{s\rho^{(f)}}{\rho^{(E)}\hat{L}\zeta}\epsilon_{pmj}\mathrm{i}k_m\breve{J}_j^{(m)} \end{pmatrix}. \tag{A-9}$$

The coefficients are given by

$$\begin{pmatrix} a_{11} & a_{12} \\ a_{21} & a_{22} \end{pmatrix} = \begin{pmatrix} s^2\rho^{(f)} & -\dfrac{s(k^2+\zeta\eta^{(e)})}{L\zeta} \\ s^2\rho + G^{(fr)}k^2 & -\dfrac{s\rho^{(f)}}{\hat{L}\rho^{(E)}\zeta}(k^2+\zeta\varsigma) \end{pmatrix}, \tag{A-10}$$

and

$$\begin{pmatrix} b_{11} & b_{12} \\ b_{21} & b_{22} \end{pmatrix} = \begin{pmatrix} C & \dfrac{s}{\hat{L}\zeta} - \dfrac{M\varsigma}{s\hat{L}\rho^{(E)}} \\ H-G^{(fr)} & \dfrac{s\rho^{(f)}}{\hat{L}\rho^{(E)}\zeta} - \dfrac{C\varsigma}{s\hat{L}\rho^{(E)}} \end{pmatrix}. \tag{A-11}$$

For later use it is convenient to also have the following combinations

$$\begin{aligned} \begin{pmatrix} c_{11} & c_{12} \\ c_{21} & c_{22} \end{pmatrix} &= \begin{pmatrix} a_{11}+b_{11}k^2 & a_{12}+b_{12}k^2 \\ a_{21}+b_{21}k^2 & a_{22}+b_{22}k^2 \end{pmatrix} \\ &= \begin{pmatrix} s^2\rho^{(f)} + Ck^2 & -\dfrac{s\eta^{(e)}}{\hat{L}} - \dfrac{M\varsigma k^2}{s\hat{L}\rho^{(E)}} \\ s^2\rho + Hk^2 & -\dfrac{s\rho^{(f)}\varsigma}{\hat{L}\rho^{(E)}} - \dfrac{C\varsigma k^2}{s\hat{L}\rho^{(E)}} \end{pmatrix}. \end{aligned} \tag{A-12}$$

APPENDIX B: MATRIX INVERSION AND GREEN'S FUNCTIONS

Let us write the matrix of equation A-8 as

$$\begin{pmatrix} \mathbf{A} & \mathbf{B} \\ \mathbf{C} & \mathbf{D} \end{pmatrix} = \begin{pmatrix} a_{11}\delta_{ij} + b_{11}k_ik_j & a_{12}\delta_{ik} + b_{12}k_ik_k \\ a_{21}\delta_{pj} + b_{21}k_pk_j & a_{22}\delta_{pk} + b_{22}k_pk_k \end{pmatrix}, \tag{B-1}$$

Then the inverse can be written as

$$\begin{pmatrix} \mathbf{A} & \mathbf{B} \\ \mathbf{C} & \mathbf{D} \end{pmatrix}^{-1} = \begin{pmatrix} \mathbf{P} & \mathbf{Q} \\ \mathbf{R} & \mathbf{S} \end{pmatrix}. \tag{B-2}$$

Because of the fact that our matrix consists of four similar symmetric square block matrices we are only interested in the expression for $\mathbf{P}$. It is given by $\mathbf{P} = (\mathbf{A} - \mathbf{B}\mathbf{D}^{-1}\mathbf{C})^{-1}$ and the other matrices can be found from this solution by substitution. The matrix of equation B-1 consists of four 3×3 block matrices. The inverse of each such block matrix is given by

$$(\alpha\delta_{ij} + \beta k_ik_j)\left[\alpha^{-1}(\delta_{jk} - \frac{\beta k_jk_k)}{\alpha+\beta k^2}\right] = \delta_{ik}, \tag{B-3}$$

where the term between square brackets in the left-hand side of the above equation denotes the inverse of the term to the left of it, which represents a block matrix. With the aid of equation B-3 $\mathbf{P}$, as expressed in equation B-2, is given in components by

$$P_{ij} = \frac{a_{22}}{a_{11}a_{22} - a_{12}a_{21}}\left(\delta_{ij} - \frac{k_i k_j}{k^2}\right) + \frac{c_{22}}{c_{11}c_{22} - c_{12}c_{21}}\frac{k_i k_j}{k^2}. \tag{B-4}$$

Notice that the division by k^2 in both expressions is only an apparent singularity and this pole will give a zero contribution in the inverse spatial Fourier transformation. The expression for $\mathbf{S}$ can be written down by interchanging subscripts $_1$ and $_2$ in the expression for $\mathbf{P}$,

$$S_{ij} = \frac{a_{11}}{a_{11}a_{22} - a_{12}a_{21}}\left(\delta_{ij} - \frac{k_i k_j}{k^2}\right) + \frac{c_{11}}{c_{11}c_{22} - c_{12}c_{21}}\frac{k_i k_j}{k^2}. \tag{B-5}$$

The expression for $\mathbf{Q}$ is obtained from $\mathbf{P}$ by keeping the second subscripts unchanged and interchanging the values $_1$ and $_2$ in the first subscripts,

$$Q_{ij} = \frac{-a_{12}}{a_{11}a_{22} - a_{12}a_{21}}\left(\delta_{ij} - \frac{k_i k_j}{k^2}\right) - \frac{c_{12}}{c_{11}c_{22} - c_{12}c_{21}}\frac{k_i k_j}{k^2}. \tag{B-6}$$

The expression for $\mathbf{R}$ is obtained from $\mathbf{P}$ by keeping the first subscripts unchanged and interchanging the values $_1$ and $_2$ in the second subscripts,

$$R_{ij} = \frac{-a_{21}}{a_{11}a_{22} - a_{12}a_{21}}\left(\delta_{ij} - \frac{k_i k_j}{k^2}\right) - \frac{c_{21}}{c_{11}c_{22} - c_{12}c_{21}}\frac{k_i k_j}{k^2}. \tag{B-7}$$

The denominators can be written as

$$\begin{aligned}\frac{1}{a_{11}a_{22} - a_{12}a_{21}} &= \frac{\hat{L}\zeta}{sG^{(fr)}}\frac{1}{(k^2 + s^2\rho/G^{(fr)})(k^2 + s^2\zeta\eta^{(e)}) - (s\rho^{(f)})^2(k^2 + \zeta\varsigma)/(\rho^{(E)}G^{(fr)})} \\ &= \frac{\hat{L}\zeta}{sG^{(fr)}}\frac{1}{(k^2 + \gamma_S^2)(k^2 + \gamma_{EM}^2)}.\end{aligned} \tag{B-8}$$

The S-wave and electromagnetic spherical wave numbers, γ_S, γ_{EM}, respectively, are found as

$$\gamma_S = \frac{1}{\sqrt{2}}\left(\frac{s^2\rho^{(c)}}{G^{(fr)}} + \zeta\eta^{(e)} + \sqrt{\left(\frac{s^2\rho^{(c)}}{G^{(fr)}} - \zeta\eta^{(e)}\right)^2 - \frac{4s^3\zeta(\rho^{(f)}\hat{L})^2}{G^{(fr)}}}\right)^{1/2}, \tag{B-9}$$

$$\gamma_{EM} = \frac{1}{\sqrt{2}}\left(\frac{s^2\rho^{(c)}}{G^{(fr)}} + \zeta\eta^{(e)} - \sqrt{\left(\frac{s^2\rho^{(c)}}{G^{(fr)}} - \zeta\eta^{(e)}\right)^2 - \frac{4s^3\zeta(\rho^{(f)}\hat{L})^2}{G^{(fr)}}}\right)^{1/2}, \tag{B-10}$$

with $\rho^{(c)} = \rho - (\rho^{(f)})^2/\rho^E$, and $\Re\{\gamma_S, \gamma_{EM}\} \geq 0$.

$$\begin{aligned}\frac{1}{c_{11}c_{22} - c_{12}c_{21}} &= \frac{s\rho^{(E)}\hat{L}/\varsigma}{HM(k^2 + s^2\rho^E\eta^{(e)}/(M\varsigma))(k^2 + s^2\rho/H) - C^2(k^2 + s^2\rho^{(f)}/C)^2} \\ &= \frac{s\rho^{(E)}\hat{L}}{\varsigma(HM - C^2)(k^2 + \gamma_{Pf}^2)(k^2 + \gamma_{Ps}^2)}.\end{aligned} \tag{B-11}$$

In this expression the spherical wave numbers of the fast and slow longitudinal waves, γ_{Pf}, γ_{Ps}, respectively, are given by

$$\gamma_{Pf} = \frac{s}{\sqrt{2}} \left(\nu - \sqrt{\nu^2 + 4\frac{(\rho^{(f)})^2 - \rho\rho^E\eta^{(e)}/\varsigma}{HM - C^2}} \right)^{1/2}, \tag{B-12}$$

$$\gamma_{Ps} = \frac{s}{\sqrt{2}} \left(\nu + \sqrt{\nu^2 + 4\frac{(\rho^{(f)})^2 - \rho\rho^E\eta^{(e)}/\varsigma}{HM - C^2}} \right)^{1/2}, \tag{B-13}$$

with $\Re\{\gamma_{Pf}, \gamma_{Ps}\} \geq 0$, and

$$\nu = \frac{\rho M - 2\rho^{(f)}C + \rho^E H\eta^{(e)}/\varsigma}{HM - C^2}. \tag{B-14}$$

We can now write the matrices as

$$\begin{aligned} P_{ij} = &-\frac{\rho^{(f)}}{\rho^{(E)}G^{(fr)}} \frac{(k^2 + \zeta\varsigma)}{(k^2 + \gamma_S^2)(k^2 + \gamma_{EM}^2)} \left(\delta_{ij} - \frac{k_i k_j}{k^2} \right) \\ &- \left(\frac{C}{HM - C^2} \right) \frac{(k^2 + s^2\rho^{(f)}/C)}{(k^2 + \gamma_{Pf}^2)(k^2 + \gamma_{Ps}^2)} \frac{k_i k_j}{k^2}, \end{aligned} \tag{B-15}$$

$$\begin{aligned} Q_{ij} = &\frac{1}{G^{(fr)}} \frac{(k^2 + \zeta\eta^{(e)})}{(k^2 + \gamma_S^2)(k^2 + \gamma_{EM}^2)} \left(\delta_{ij} - \frac{k_i k_j}{k^2} \right) \\ &+ \left(\frac{M}{HM - C^2} \right) \frac{(k^2 + s^2\rho^{(E)}\eta^{(e)}/(M\varsigma))}{(k^2 + \gamma_{Pf}^2)(k^2 + \gamma_{Ps}^2)} \frac{k_i k_j}{k^2}, \end{aligned} \tag{B-16}$$

$$\begin{aligned} R_{ij} = &-\frac{\hat{L}\zeta}{s} \frac{(k^2 + s^2\rho/G^{(fr)})}{(k^2 + \gamma_S^2)(k^2 + \gamma_{EM}^2)} \left(\delta_{ij} - \frac{k_i k_j}{k^2} \right) \\ &- \left(\frac{Hs\rho^{(E)}\hat{L}}{(HM - C^2)\varsigma} \right) \frac{(k^2 + s^2\rho/H)}{(k^2 + \gamma_{Pf}^2)(k^2 + \gamma_{Ps}^2)} \frac{k_i k_j}{k^2}, \end{aligned} \tag{B-17}$$

$$\begin{aligned} S_{ij} = &\frac{s\rho^{(f)}\hat{L}\zeta}{G^{(fr)}} \frac{1}{(k^2 + \gamma_S^2)(k^2 + \gamma_{EM}^2)} \left(\delta_{ij} - \frac{k_i k_j}{k^2} \right) \\ &+ \left(\frac{Cs\rho^{(E)}\hat{L}}{(HM - C^2)\varsigma} \right) \frac{(k^2 + s^2\rho^{(f)}/C)}{(k^2 + \gamma_{Pf}^2)(k^2 + \gamma_{Ps}^2)} \frac{k_i k_j}{k^2}. \end{aligned} \tag{B-18}$$

From the fact that $k = 0$ gives a zero contribution we find the following identity from the matrix $\mathbf{P}$ as

$$\left(\frac{\gamma_{Ps}\gamma_{Pf}}{\gamma_S\gamma_{EM}} \right)^2 = \frac{s^2\rho^{(E)}G^{(fr)}}{(HM - C^2)\zeta\varsigma}, \tag{B-19}$$

which is easily verified to be correct. The same result is obtained from taking $k = 0$ in any of the other matrices. It can also be used to check results of Green's functions that are linear combinations of these matrices. The Green's functions for the particle velocity and

the electric field of equation 12 can be written in terms of the four matrices as

$$\breve{G}^{vf}_{ij} = sQ_{ij}, \tag{B-20}$$

$$\breve{G}^{ve}_{ir} = \frac{P_{ij}(s^2\rho^{(E)}\delta_{jr} + Mk_jk_r) + Q_{ij}(s^2\rho^{(f)}\delta_{jr} + Ck_jk_r)}{s\rho^{(E)}\hat{L}}, \tag{B-21}$$

$$\breve{G}^{vff}_{ij} = sP_{ij}, \tag{B-22}$$

$$\breve{G}^{vm}_{ip} = -\frac{(s\rho^{(E)}P_{ij} + s\rho^{(f)}Q_{ij})\epsilon_{jmp}\mathrm{i}k_m}{\rho^{(E)}\hat{L}\zeta}, \tag{B-23}$$

$$\breve{G}^{vq}_{i} = (MP_{ij} + CQ_{ij})\mathrm{i}k_j, \tag{B-24}$$

$$\breve{G}^{vh}_{ikl} = (CP_{ij} + (H - 2G^{(fr)})Q_{ij})\mathrm{i}k_j\delta_{kl} + 2G^{(fr)}Q_{ik}\mathrm{i}k_l, \tag{B-25}$$

and

$$\breve{G}^{ef}_{ij} = sS_{ij}, \tag{B-26}$$

$$\breve{G}^{ee}_{ir} = \frac{R_{ij}(s^2\rho^{(E)}\delta_{jr} + Mk_jk_r) + S_{ij}(s^2\rho^{(f)}\delta_{jr} + Ck_jk_r)}{s\rho^{(E)}\hat{L}}, \tag{B-27}$$

$$\breve{G}^{eff}_{ij} = sR_{ij}, \tag{B-28}$$

$$\breve{G}^{em}_{ip} = -\frac{(s\rho^{(E)}R_{ij} + s\rho^{(f)}S_{ij})\epsilon_{jmp}\mathrm{i}k_m}{\rho^{(E)}\hat{L}\zeta}, \tag{B-29}$$

$$\breve{G}^{eq}_{i} = (MR_{ij} + CS_{ij})\mathrm{i}k_j, \tag{B-30}$$

$$\breve{G}^{eh}_{ikl} = (CR_{ij} + (H - 2G^{(fr)})S_{ij})\mathrm{i}k_j\delta_{kl} + 2G^{(fr)}S_{ik}\mathrm{i}k_l. \tag{B-31}$$

By comparing equation B-31 with equations B-26 and B-28 it can be seen that the electric field generated by a deformation rate source can be written by two moment tensors, one for the responses of a force source acting on the bulk and one for a force source acting on the fluid. Incorporation of a deformation source as a source term gives a contribution $CR_{ij}\mathrm{i}k_j\delta_{kl}$ that is not included in the response given by Gao and Hu (2010). This has an effect on the derived responses for other field quantities. All other Green's functions can be found from these sets and the basic equations. All Green's functions are explicitly given in the main text. For notational convenience we give the expressions for the scalar Green's functions for transversal $\breve{G}^{SS}$ and longitudinal waves $\breve{G}^{PP}$ as

$$\breve{G}^{SS} = \frac{\gamma^2_{EM} - \gamma^2_S}{(k^2 + \gamma^2_S)(k^2 + \gamma^2_{EM})} = \frac{1}{k^2 + \gamma^2_S} - \frac{1}{k^2 + \gamma^2_{EM}}, \tag{B-32}$$

$$\breve{G}^{PP} = \frac{\gamma^2_{Ps} - \gamma^2_{Pf}}{(k^2 + \gamma^2_{Pf})(k^2 + \gamma^2_{Ps})} = \frac{1}{k^2 + \gamma^2_{Pf}} - \frac{1}{k^2 + \gamma^2_{Ps}}. \tag{B-33}$$

These are used in the main text for ease of notation that can be used in space-frequency domain as well.

APPENDIX C: TRANSFORMATION BACK TO SPACE-FREQUENCY DOMAIN

Every scalar part of the Green's functions given in equations 13-22 can be written in the form,

$$\breve{H}(k,s) = \frac{\breve{F}(k,s)}{k^2+\gamma_a^2}, \tag{C-1}$$

with $\breve{F}(k,s)$ a regular function consisting of the prefactor of the total Green's function in question and in which only even powers of k occur. Because the pole at $k=0$ gives a zero contribution the functions $\breve{F}$ can be considered regular functions of k. The three-dimensional inverse spatial-Fourier transform is then given by,

$$\hat{H}(\boldsymbol{x},s) = \frac{1}{(2\pi)^3}\int_{\boldsymbol{k}} \exp(-\mathrm{i}\boldsymbol{k}\cdot\boldsymbol{x})\breve{H}(\boldsymbol{k},s)\mathrm{d}^3\boldsymbol{k}. \tag{C-2}$$

Because $\breve{H}$ is a function of k only, we change to spherical coordinates in $\boldsymbol{k}$-space with center at $\boldsymbol{k}=0$ and take the direction of $\boldsymbol{x}$ as polar axis. We had already defined $k=|\boldsymbol{k}|$, we take θ as the angle between $\boldsymbol{k}$ and $\boldsymbol{x}$, and ϕ as the angle between the projection of $\boldsymbol{k}$ onto the plane perpendicular to $\boldsymbol{x}$ and some fixed direction of reference in this plane. Then the ranges of integration become $0<k<\infty$, $0<\theta<\pi$ and $0<\phi<2\pi$, with

$$\boldsymbol{k}\cdot\boldsymbol{x} = k|\boldsymbol{x}|\cos(\theta), \quad \boldsymbol{k}\cdot\boldsymbol{k}=k^2, \quad \mathrm{d}^3\boldsymbol{k} = \mathrm{k}^2\sin(\theta)\mathrm{dk}\mathrm{d}\theta\mathrm{d}\phi. \tag{C-3}$$

The integration with respect to ϕ amounts to multiplication by 2π, and the integration with respect to θ results in

$$\hat{H}(\boldsymbol{x},s) = \frac{1}{4\pi^2|\boldsymbol{x}|\mathrm{i}}\int_{k=0}^{\infty}\frac{\exp(\mathrm{i}k|\boldsymbol{x}|)-\exp(-\mathrm{i}k|\boldsymbol{x}|)}{k^2+\gamma_a^2}\breve{F}(k,s)k dk, \tag{C-4}$$

Notice that the negative exponent can be dropped if the lower integration limit is extended to $-\infty$, because in $\breve{F}$ no odd powers of k occur,

$$\hat{H}(\boldsymbol{x},s) = \frac{1}{4\pi^2|\boldsymbol{x}|\mathrm{i}}\int_{k=-\infty}^{\infty}\frac{\exp(\mathrm{i}k|\boldsymbol{x}|)}{k^2+\gamma_a^2}\breve{F}(k,s)k dk. \tag{C-5}$$

If now the path of integration is supplemented with a semicircle situated in the upper half-plane with an infinite radius, such that a counter-clockwise closed path of integration is obtained, the residue theorem can be applied. Jordan's Lemma shows that the contribution from the semicircle vanishes at infinity, therefore the outcome of the closed path integral is the same as that of equation C-5. According to the residue theorem $\hat{H}(\boldsymbol{x},s)$ is equal to $2\pi\mathrm{i}$ times the residue of the simple pole of $\breve{H}(k,s)$, and the residue of the pole is given by,

$$\mathrm{Res}_{k=\mathrm{i}\gamma_a}\left(\breve{H}(k,s)\right) = \lim_{k\to\mathrm{i}\gamma_a}\frac{1}{4\pi^2|\boldsymbol{x}|\mathrm{i}}\frac{\exp(\mathrm{i}k|\boldsymbol{x}|)(k-\mathrm{i}\gamma_a)k}{(k+\mathrm{i}\gamma_a)(k-\mathrm{i}\gamma_a)}\breve{F}(k,s) \tag{C-6}$$

$$= \frac{1}{4\pi^2|\boldsymbol{x}|\mathrm{i}}\frac{\exp(-\gamma_a|\boldsymbol{x}|)\mathrm{i}\gamma_a}{2\mathrm{i}\gamma_a}\breve{F}(\mathrm{i}\gamma_a,s) \tag{C-7}$$

$$= \frac{\exp(-\gamma_a|\boldsymbol{x}|)}{8\pi^2|\boldsymbol{x}|\mathrm{i}}\hat{F}(\mathrm{i}\gamma_a,s), \tag{C-8}$$

leading to

$$\hat{H}(\boldsymbol{x},s)=\hat{F}(\mathrm{i}\gamma_a,s)\frac{\exp(-\gamma_a|\boldsymbol{x}|)}{4\pi|\boldsymbol{x}|}. \tag{C-9}$$

In the rest of the Green's function expressions the $\boldsymbol{k}$-dependent factors are of the form $-\mathrm{i}k_i$ and k_ik_j/k^2 and lead to spatial derivatives ∂_i and $\gamma_W^{-2}\partial_i\partial_j$ after transformation. In the last expression W refers to the wave type, which can be $W=\{Pf,Ps,S,EM\}$. From equations 13-22 we observe that up to four gradients for a Green's function of wave type W must be evaluated,

$$\hat{G}^W(\boldsymbol{x},\boldsymbol{x}^s,s)=\frac{\exp(-\gamma_W R)}{4\pi R}, \tag{C-10}$$

in which R is the source-receiver distance $R=|\boldsymbol{x}-\boldsymbol{x}^s|>0$.

If we take one to four gradients we obtain

$$\partial_r\hat{G}^W(\boldsymbol{x},s)=-\left(\frac{1}{R}+\gamma_W\right)\frac{x_k}{R}\frac{\exp(-\gamma_W R)}{4\pi R}, \tag{C-11}$$

$$\partial_k\partial_r\hat{G}^W(\boldsymbol{x},s)=\left[\left(3\frac{x_kx_r}{R^2}-\delta_{kr}\right)\left(\frac{1}{R^2}+\frac{\gamma_W}{R}\right)+\frac{x_kx_r}{R^2}\gamma_W^2\right]\frac{\exp(-\gamma_W R)}{4\pi R}, \tag{C-12}$$

$$\begin{aligned}\partial_m\partial_k\partial_r\hat{G}^W(\boldsymbol{x},s)=&\left[\frac{\delta_{mk}x_r+\delta_{mr}x_k+\delta_{kr}x_m}{R}\left(\frac{3}{R^3}+\frac{3\gamma_W}{R^2}+\frac{\gamma_W^2}{R}\right)\right.\\&\left.-\frac{x_mx_kx_r}{R^3}\left(\frac{15}{R^3}+\frac{15\gamma_W}{R^2}+\frac{6\gamma_W}{R}+\gamma_W^3\right)\right]\frac{\exp(-\gamma_W R)}{4\pi R},\end{aligned} \tag{C-13}$$

$$\begin{aligned}\partial_n\partial_m\partial_k\partial_r\hat{G}^W(\boldsymbol{x},s)=&\left[(\delta_{mk}\delta_{nr}+\delta_{mr}\delta_{nk}+\delta_{kr}\delta_{mn})\left(\frac{3}{R^4}+3\frac{\gamma_W}{R^3}+\frac{\gamma_W^2}{R^2}\right)\right.\\&-\frac{\delta_{nm}x_kx_r+\delta_{nk}x_mx_r+\delta_{nr}x_mx_k+\delta_{mk}x_nx_r+\delta_{mr}x_nx_k+\delta_{kr}x_nx_m}{R^2}\\&\times\left(\frac{15}{R^4}+15\frac{\gamma_W}{R^3}+6\frac{\gamma_W^2}{R^2}+\frac{\gamma_W^3}{R}\right)\\&\left.+\frac{x_nx_mx_kx_r}{R^4}\left(\frac{105}{R^4}+105\frac{\gamma_W}{R^3}+45\frac{\gamma_W^2}{R^2}+10\frac{\gamma_W^3}{R}+\gamma_W^4\right)\right]\frac{\exp(-\gamma_W R)}{4\pi R}.\end{aligned} \tag{C-14}$$

For the Green's functions we define six tensor Green's functions with which we can write all fields generated by any source,

$$\hat{G}_i^W(\boldsymbol{x},s)=\partial_i\hat{G}^W(\boldsymbol{x},s), \tag{C-15}$$

$$\hat{\mathcal{G}}_{ij}^W(\boldsymbol{x},s)=\gamma_W^{-2}\partial_i\partial_j\hat{G}^W(\boldsymbol{x},s), \tag{C-16}$$

$$\hat{G}_{ij}^W(\boldsymbol{x},s)=\hat{\mathcal{G}}_{ij}^W(\boldsymbol{x},s)-\delta_{ij}\hat{G}^W(\boldsymbol{x},s), \tag{C-17}$$

$$\hat{G}_{ijk}^W(\boldsymbol{x},s)=\gamma_W^{-2}\partial_i\partial_j\partial_k\hat{G}^W(\boldsymbol{x},s)-\delta_{ij}\hat{G}_k^W(\boldsymbol{x},s), \tag{C-18}$$

$$\hat{\mathcal{G}}_{ijkl}^W(\boldsymbol{x},s)=\gamma_W^{-2}\partial_i\partial_j\partial_k\partial_l\hat{G}^W(\boldsymbol{x},s)-\delta_{ij}\partial_k\partial_l\hat{G}^W(\boldsymbol{x},s), \tag{C-19}$$

$$\hat{G}_{ijkl}^W(\boldsymbol{x},s)=\frac{\partial_i\partial_j\partial_k\partial_l\hat{G}^W(\boldsymbol{x},s)}{\gamma_W^4}-\frac{(\delta_{ij}\partial_k\partial_l+\partial_i\partial_j\delta_{kl})\hat{G}^W(\boldsymbol{x},s)}{\gamma_W^2}+\delta_{ij}\delta_{kl}\hat{G}^W(\boldsymbol{x},s). \tag{C-20}$$

With these results and expressions for the gradients we can find all space domain Green's functions and these are given in the main text.

Table 1: Medium parameters, symbols, values, and SI units.

Parameter	Symbol	value	SI unit
free space permittivity	ε_0	8.854×10^{-12}	s/(Ωm)
free space permeability	μ_0	$4\pi \times 10^{-7}$	sΩ/m
bulk electric permittivity	ε	$11.6\varepsilon_0$	s/(Ωm)
bulk magnetic permeablity	μ	μ_0	sΩ/m
bulk electric conductivity	$\sigma^{(e)}$	9.3×10^{-4}	S/m
bulk magnetic conductivity	$\sigma^{(m)}$	0	Ω/m
viscosity	η	10^{-3}	kg/(sm)
static permeability	k_0	1.3×10^{-12}	m^2
tortuosity	α_∞	3	-
porosity	ϕ	0.38	-
shear modulus	$G^{(fr)}$	9×10^9	N/m^2
bulk modulus	K_G	9.35×10^9	N/m^2
fluid density	$\rho^{(f)}$	1000	kg/m^3
bulk density	ρ	2190	kg/m^3
coupling coefficient	L	6.8×10^{-9}	m^2s/V